Published in final edited form as:
Chemphyschem. 2014 November 10; 15(16): 3572–3579. doi:10.1002/cphc.201402354.

Investigating the thermostability of succinate: quinone oxidoreductase enzymes by direct electrochemistry at SWNTs-modified electrodes and FTIR spectroscopy

Frederic Melin[a], **Mohamed R. Noor**[b], **Elodie Pardieu**[c], **Fouzia Boulmedais**[c,d,e], **Florian Banhart**[f], **Gary Cecchini**[g], **Tewfik Soulimane**[b], and **Petra Hellwig**[a]

Petra Hellwig: hellwig@unistra.fr

[a]Laboratoire de Bioélectrochimie et Spectroscopie Chimie de la Matière Complexe (UMR 7140) Université de Strasbourg 1 Rue Blaise Pascal, 67000 Strasbourg (France) [b]Chemical and Environmental Sciences Department & Materials and Surface Science Institute University of Limerick Limerick, Ireland [c]Institut Charles Sadron, CNRS UPR 22 Université de Strasbourg 23 rue du Loess, BP 84047, 67034 Strasbourg Cedex 2 (France) [d]International Center for Frontier Research in Chemistry 8 allée Gaspard Monge, 67083 Strasbourg (France) [e]Institut d'Etudes Avancées de l'Université de Strasbourg 5 allée du Général Rouvillois, 67083 Strasbourg (France) [f]Institut de Physique et Chimie des Matériaux de Strasbourg Université de Strasbourg, UMR 7504 CNRS 23 rue du Loess, 67034 Strasbourg (France) [g]Molecular Biology Division, Veterans Affairs Medical Center San Francisco, California 94121, and Department of Biochemistry and Biophysics, University of California, San Francisco, California 94158

Abstract

Succinate Quinone reductases (SQRs) are the enzymes which couple the oxidation of succinate and the reduction of quinones in the respiratory chain of prokaryotes and eukaryotes. We compare herein the temperature-dependent activity and structural stability of two SQRs, the first one from the mesophilic bacterium E. coli and the second one from the thermophilic bacterium T. thermophilus by a combined electrochemical and infrared spectroscopy approach. Direct electron transfer was achieved with the full membrane protein complexes at SWNTs-modified electrodes. The possible structural factors which contribute to the temperature-dependent activity of the enzymes and to the thermostability of the T. thermophiles SQR in particular, are discussed.

Keywords

membrane proteins; succinate:quinone oxidoreductase; carbon nanotubes; protein film voltammetry; IR spectroscopy; thermostability

Correspondence to: Petra Hellwig, hellwig@unistra.fr.

Supporting information for this article is available on the WWW under http://www.chemphyschem.org or from the author

1. Introduction

Succinate: quinone oxidoreductases (SQRs) are membrane proteins that couple the oxidation of succinate to fumarate and the reduction of quinone into quinol in aerobic respiration processes. They are related to quinol: fumarate oxidoreductases (QFRs) which catalyze the reverse reaction in anaerobic respiration processes using fumarate as the terminal electron acceptor. Both type of enzymes belong to the succinate:quinone oxidoreductase (SQOR) superfamily and are also known as respiratory complex II due to their location within the electron transport chain.[1–8] SQORs usually comprise two hydrophilic subunits A and B, which are highly conserved, and either one large (C) or two small (C and D) membrane-bound subunits. Succinate binds in the hydrophilic subunit A close to a flavin adenine dinucleotide (FAD) cofactor whereas the quinone molecule binds in the membrane part of the enzyme. A chain of three iron-sulfur clusters located in the hydrophilic part (one each of [2Fe-2S], [4Fe-4S] and [3Fe-4S]) allows the transfer of electrons between both sites. Depending on the organism, the number of heme b moieties in the membrane domain of the enzyme can range from zero to two. The role of these additional cofactors is still not very clear at present. A well-accepted classification of SQORs has been established, based on the number of membrane-bound domains as well as heme *b* content. Type B SQORs contain only one membrane domain, while type A, C, D and E contain two membrane-bound domains. Type D and E contain zero, type C one and type A and B two hemes b in their membrane part. Fully characterized SQORs include D-type QFR from *Escherichia coli*,[9] B-type QFR from *Wollinella succinogenes*,[10] C-type SQRs from *E. coli*,[11–13] avian heart[14] and porcine heart.[15] More recently, an extensive characterization of a type-A SQOR, the SQR from the extremophilic bacterium *Thermus thermophilus*,[16, 17] was reported. This enzyme exhibits atypical features, including high thermostability, and an optimum of activity at 70 °C. In its native form, this SQR is found in a trimeric state and cooperativity between the protomers has been demonstrated at high temperature. A recombinant form of the enzyme bearing a His-tag protruding into the trimerization contact point preventing oligomerization has been also prepared. This artificially-produced monomeric form of *T. thermophilus* SQR also exhibits an increase in turnover between 30 and 70 °C despite an unchanged affinity for succinate.[17] The methods by which thermophilic proteins achieve thermostability have been the subject of various investigations,[18–22] although it was not discussed in much details in the case of SQR from *T. thermophilus*. From the comparison of sequences and structures of several thermophilic proteins with their mesophilic homologues, several factors which contribute to higher thermal stability have been identified including: (i) a reduction of mobile surface loops and turns, (ii) a strengthening of the hydrophobic core of the protein and (iii) an increased occurrence of internal salt bridges. These structural modifications either reduce the conformational disorder of the protein or increase the enthalpy difference between their folded and unfolded states.

Catalytic activity of SQORs can be probed by direct protein film voltammetry on pyrrolitic graphite electrodes (PGE). For this approach, it is necessary that the enzymes retain their native properties upon immobilization and the interfacial electron transfer between the electrode and the redox-active cofactors must not be limiting. Reported studies so far have

concerned mainly hydrophilic domains of SQORs such as succinate dehydrogenases (SDH) from *E. coli*[23] and beef heart,[24] and fumarate reductases (FRD) from *E. coli*[25–27] and *Shewanella frigidimarina*.[28] Despite the limited stability over time of the films and sometimes low coverage of the electrode with electroactive enzymes, these systems exhibit an interesting electrocatalytic behavior. It was observed that immobilized SDHs or FRDs remain fully active in both oxidation of succinate and reduction of fumarate. The activity of SDHs in fumarate reduction, however, displays an atypical dependence on the applied potential. The catalytic current first increases when the potential is scanned towards cathodic potentials and then drops significantly at lower potentials (i.e; higher electrochemical driving force). This unusual behavior, which allows for the differentiation of SDHs from FRDs, is not fully understood yet. Recently Kolaj-Robin et al. reported the electrochemical analysis at relatively high temperature of the full SQOR complex from *T. thermophilus* immobilized on PGE.[16] This report prompted us to study and compare the temperature-dependent electrochemical behavior of the full SQR complex from the mesophilic bacterium *E. coli*, which is believed to be a functional monomer in solution, and of the recombinant monomeric SQR variant from the thermophilic bacterium *T. thermophilus*. Both enzymes share a similar molecular weight (120 kDa). To optimize the protein coverage on the electrode surface, we have increased the specific surface area of the electrode by deposition of single-walled carbon nanotubes (SWNTs). The mixed SWNTs/ protein films were characterized by resonance Raman spectroscopy and atomic force microscopy (AFM). FTIR spectroscopy allowed us to discuss the conformational and secondary structure alterations in the proteins which occur upon electron transfer and upon heating.

2. Results and Discussion

2.1 Electrochemically-Induced FTIR Difference Spectroscopy

Redox-driven changes in the environment of the FAD, heme groups, and polypeptide backbone as well as protonation changes of individual amino acid residues can be determined by FTIR difference spectroscopy. The oxidized-minus-reduced difference spectra obtained for *E. coli* and monomeric variant of *T. thermophilus* SQRs for a potential step from −0.40 V to 0.20 V (vs SHE) at pH 8 are shown in Figure 1. The positive signals thus belong to the oxidized state of the protein whereas the negative signals belong to the reduced state. The proposed attribution of the signals is based on previous studies on related QFR from *E. coli*[29] and *W. succinogenes*,[30, 31] as well as other FAD-containing proteins[32, 33] and heme *b*-containing proteins.[34, 35] The spectra exhibit some obvious similarities, as could be expected from the similar secondary structure and cofactor content of both enzymes.

Polypeptide backbone contributions: a major differential feature can be seen in both spectra between 1680 and 1630 cm^{-1}, which involve the C=O stretching vibrations of the polypeptide chain (the so-called amide I region). These signals are often observed in iron-sulfur proteins and correspond to the reorganization of the backbone upon electron transfer to the clusters.[29, 36, 33] In particular the strong negative signal at 1656-1568 cm^{-1} can be attributed to the predominant contribution of the α-helices whereas the signals in the 1620–

1630 cm^{-1} correspond to the β-sheets. Signals between 1570 and 1520 cm^{-1} (amide II region) include C-N stretching and N-H bending vibration of the polypeptide backbone.

Cofactor contributions: the oxidized FAD cofactor exhibits distinctive signals at 1711 ($\upsilon(C_4=O)$), 1673 ($\upsilon(C_2=O)$) and 1548 cm^{-1} ($\upsilon(C=N)$) at pH 8.[32, 33] The first signal is found at 1711 cm^{-1} in *T. thermophilus* SQR and at 1706 cm^{-1} in *E coli* SQR, which suggests that the FAD are in different hydrogen-bond environment in these proteins. The $\upsilon(C=N)$ vibrations of the flavin probably contributes to the strong signal at 1536 cm^{-1} observed for both proteins. Signals of the reduced form of the flavin are expected in the 1630-1550 cm^{-1} region ($\upsilon(C=O)/\upsilon(C=C$ modes)), and at 1520 ($\delta(C-H)/\delta(N-H)$ mode) and 1410 cm^{-1} (isoalloxazine ring reorganization). This latter mode probably contributes to the signal observed at 1404 cm^{-1} in the *T. thermophilus* SQR and at 1398 cm^{-1} in its *E. coli* counterpart. The heme *b* porphyrin vibrations exhibit a series of signals which also largely overlap with the amide I and amide II bands. However, the strong bands observed in the reduced state of heme *b*-containing proteins in the 1560-1540 cm^{-1} region are usually assigned to the υ_{37} (C_bC_b) and υ_{38} (C_aC_m) skeletal porphyrin modes. These modes are observed here at 1557 and 1548 cm^{-1} for the *T. thermophilus* enzyme and its *E. coli* counterpart respectively. The heme propionates exhibit signals in the 1700-1660 cm^{-1} region when protonated and in the 1620-1540 cm^{-1} (υ_{as} COO^-) and 1420-1300 cm^{-1} (υ_s COO^-) regions when deprotonated. These modes, however, are very difficult to assign unequivocally here because they overlap with the polypeptide backbone, and flavin contributions. They probably contribute to the positive signals observed at 1591 and 1571 cm^{-1} in the oxidized state of the *T. thermophilus* enzyme and at 1586 cm^{-1} in its *E. coli* homologue.

Individual amino acids contributions: The $\upsilon(C=O)$ modes of protonated aspartic and glutamic acid side chains are expected in the 1800-1710 cm^{-1}spectral range.[37–39] Beside the band at 1706 cm^{-1} due to the FAD cofactor, no significant difference signal can be observed for the *E. coli* enzyme, whereas a clear signal is observed at 1731 cm^{-1} for the reduced state of the *T. thermophilus* enzyme. We can thus conclude that an acidic residue in a highly hydrophobic environment is protonated upon reduction of the enzyme. The deprotonated aspartic and glutamic acid residues probably contribute also to the bands observed in the 1590-1571 cm^{-1} region for the oxidized state and in the 1410-1400 cm^{-1} region for the reduced state. Arginines and tyrosines are expected to contribute to the signals observed at 1669 cm^{-1} and 1515 cm^{-1} respectively. For a summary of tentative assignments, see table S1 in Supporting Information.

2.2 Electrochemistry

Electrode preparation and characterization: CNTs are considered as promising supports for the immobilization and electrochemical study of proteins[40–50] because of their high electrical conductivity[51] and high specific surface.[52] Membrane proteins in particular should adsorb easily on the hydrophobic sidewalls of these carbon nanomaterials. Hence, we have modified a commercial glassy carbon disk electrode by drop-casting of a dispersion of SWNTs in $EtOH/H_2O$ mixture. The electrode was then annealed at 100 °C for 2 hours to improve the stability of the carbon nanotubes layer. For protein adsorption, it was necessary

to decrease the concentration of detergent in the samples to less than 0.05 %. Adsorption was then performed by direct incubation of the electrode surface with the solution of protein overnight at 4 °C. The SQR/CNTs assemblies were characterized by resonance Raman spectroscopy (Figure S1 in Supporting Information). The CNTs exhibit several bands in the available range which can be easily identified.[53, 54] The strong band at 1580 cm^{-1} (the G-band) corresponds to the tangential vibrations of the carbon atoms. The low intensity of the band at 1340 cm^{-1} (the D-band) suggests that the carbon sp^2 network of the CNTs used here contains few defects. The signals at 100–250 cm^{-1} correspond to the radial breathing modes of the tubes and depend on the diameters of the tubes. The most prominent signals are observed at 262, 204, 188 and 158 cm^{-1} which correspond to SWNTs of 0.9, 1.1, 1.2 and 1.5 nm diameter respectively. The last band at 2670 cm^{-1} (the G' band) is a second-order harmonic band which is also dependent on the diameters of the tubes. Upon immobilization of SQR from *T. thermophilus*, characteristic heme marker bands can be observed, including υ_3 and υ_4 at 1493 and 1360 cm^{-1} respectively.[55–57] The position of these bands is characteristic of low-spin six-coordinated hemes. Other characteristic signals are observed at 2935 and 2960 cm^{-1} (υ(C-H)), 321 and 346 cm^{-1} (υ(Fe-S)).[58–62]

AFM measurements were performed to characterize the topography of the SQR/SWNT assemblies deposited on a glassy carbon substrate. The bare glassy carbon substrate has a roughness of 4 ± 1 nm. After deposition of SWNTs, an increase of the surface roughness is observed up to 63 ± 12 nm with large peaks extending over almost 200 nm in height and 1 μm in width (Figure 2A). When *E. coli* and *T. thermophilus* SQRs are deposited on SWNTs-coated substrates, the roughness decreases until 2.2 ± 0.2 nm and 4.3 ± 0.4 nm, respectively (Figure 2B and 2C). In the case of *E. coli* SQR, the topography is homogeneous and grainy. The SWNTs are completely coated by the immobilized enzyme. In the case of *T. Thermophilus SQR*, the profile is similar to that of SWNTs-coated substrate with peaks extending over almost 15 nm in height and 1 μm in width. The enzyme deposited layer seems to follow the distribution of SWNTs on the substrate suggesting that a smaller quantity of enzyme is adsorbed on the nanotubes surface in this case.

Electrocatalytic activity: the electrocatalytic activity of the immobilized SQRs was probed at pH 8 to improve the solubility of sodium succinate in water. The substrate concentration was maintained at 4 mM, well above the K_M values which was reported to be 71 μM for the *E. coli* SQR at 25 °C[63] and about 300 μM for the monomeric variant of *T. thermophilus* SQR at 30 °C and 70 °C.[17] In these conditions, the bare CNT electrode does not show any signal (see Figure 3). Both enzymes, however, exhibit a catalytic signal in presence of succinate at 20°C when immobilized on the carbon nanotubes surface. The catalytic potentials are observed at 0.00 V and 0.04 V for the *T. thermophilus* and *E. coli* SQR respectively and are thus close to the midpoint potential of the succinate/fumarate couple (−0.03 V at pH 8). Comparison of the catalytic currents clearly shows that the electrodes modified with the *T. thermophilus* SQR are more efficient in succinate oxidation than those modified with the *E. coli* SQR. This observation was not expected, because both the surface coverage (see AFM study) and the turnover rates in solution are more favorable in the case of the *E. coli* enzyme. The kinetic constants indeed were reported to be 6100 (± 5 %) and 760 (± 1 %) min^{-1} at 30°C for the *E. coli*[64] and *T. thermophilus*[17] SQRs respectively. A significant

fraction of the immobilized *E. coli* SQRs thus seem to be electrochemically inactive, either because they are not properly oriented on the surface or because they are denatured. Previous studies with soluble fragments of *E. coli* SQRs and QFRs often mentioned the low stability of the protein films.[25, 23] Decrease of protein concentration or incubation time does not lead to better electrochemical signals (See figure S2 in Supporting Information). Interestingly, the *T. thermophilus* enzyme also exhibits a small peak on the reverse scan at −0.07 V, which can be attributed to the reaction with fumarate produced on the forward scan and trapped in the carbon nanotubes matrix.

Temperature dependence: The influence of temperature on the electrocatalytic properties of the immobilized enzymes is shown in Figure 4. In the case of *E. coli* (A), a threefold increase of the catalytic current is observed between 10 and 30 °C. Between 30 and 40 °C, the activity remains almost stable but then decreases rapidly at higher temperatures. These results are consistent with the optimum temperature growth of *E. coli* which is 37 °C. For *T. thermophilus*, in contrast, a dramatic increase in activity is observed between 10 and 60 °C. The maximum current at 60 °C is approximately 10 times of that measured at 10 °C and remains stable even after incubation of the electrode at 60 °C for 30 minutes. Upon further increase in temperature, the activity eventually decreases. As compared to studies in solution which reported a peak of activity at 70 °C close to the optimum temperature growth of the enzyme,[17] SQR from *T. thermophilus* only exhibits a slight decrease of thermostability when immobilized on the carbon nanotubes surface. The temperature-dependent activity of both enzymes can be therefore reproduced quite accurately after immobilization on these carbon nanomaterials.

2.3 Temperature-dependent FTIR Spectroscopy

The structural and conformational changes occurring in the enzymes upon increasing the temperature were monitored by FTIR spectroscopy. The most relevant band for this study is the so-called amide I band in the 1700-1600 cm^{-1} range which involves for 80 % the υ(C=O) modes of the polypeptide backbone.[65–68, 39] Since water also exhibits a strong contribution in this region, the studies were performed in deuterated water. Upon exchanging H_2O by D_2O, deuteration of the protein occurs. The extent of deuteration can be followed by looking at the residual amide II band between 1600 and 1500 cm^{-1}. This band derives from the in plane N-H bending vibrations coupled to the υ(C-N) stretching vibrations and it shifts to 1450 cm^{-1} upon deuteration.

At 10 °C, the amide I band of the *E. coli* SQR (see Figure 5 and Figure S5 in Supporting Information) exhibits a maximum absorbance at 1653 cm^{-1} which is consistent with the predominant contribution of the α-helices in this enzyme. This is confirmed by the distribution of secondary-structure elements which can be obtained after deconvolution of the band (see table 1). Only minor changes are observed in the amide I region between 10 and 50 °C. Small conformational reorganizations, providing a better access of D_2O to the protein inner core, yet probably occurs, as suggested by the decrease of the residual amide II band (see Figure S3 in Supporting Information). After 50°C, however, the maximum absorbance of the amide I band shifts to lower wavenumbers and a shoulder appears at 1620 cm^{-1}. This band is usually observed when extended structures are produced after protein

denaturation and aggregation.[69–71] At 80 °C the amide I band is centered at 1645 cm^{-1} and the secondary structure analysis reveals a significant decrease in the contributions of α-helices concomitant with an increase in the contribution of β-sheets and random structures. At this temperature, the amide II band is also completely lost. The *E. coli* enzyme thus undergoes a major structural change above 50 °C which provides a full access of the solvent to the protein core. The decrease in activity observed at 50 °C correlates well with this structural alteration of the protein.

T. thermophilus SQR exhibits a predominant contribution of α-helices as well (see Figure 6 and Table 1). The distribution of secondary-structure elements obtained for this enzyme at 10 °C is consistent with a previous circular dichroism study.[17] Interestingly, the contribution of turns seems smaller for this protein than for its *E. coli* homologue. The reduction of exposed turns decreases the conformational disorder of the protein and thus contributes to the higher thermal stability of the protein.[72] In contrast with the *E. coli* enzyme, no major changes are observed in the amide I region in all the available thermal range (10–80 °C). The secondary structure elements of the enzyme at 10 °C are indeed almost conserved at 80 °C. The amide II band (see Figure S4 in Supporting Information) continuously decreases between 10 and 80 °C suggesting that small conformational changes are occurring, but contrary to the *E. coli* enzyme, this band does not completely disappears at 80 °C. Therefore, even at 80 °C, a hydrophobic core not accessible to the D_2O still remains in the *T. thermophilus* protein. As compared to the *E. coli* enzyme, the *T. thermophilus* SQR clearly exhibits a stronger hydrophobic core, which contributes as well to the higher thermal stability of this enzyme.

3. Conclusion

Immobilization of full SQR complexes on carbon nanotubes modified electrodes allowed us to study their temperature-dependent electrocatalytic activity. In the case of *E. coli* an optimum of activity was observed between 30 and 40 °C whereas for *T. thermophilus,* activity increases until 60 °C and then decreases at higher temperature. These results are consistent with the optimal temperature growth of 37 °C and 70 °C for *E. coli* and *T. thermophilus*,[73] respectively. The electrochemical studies also showed that immobilized *T. thermophilus* enzyme is more efficient in succinate oxidation than *E. coli* SQR.

The redox-induced FTIR difference spectroscopy reveals the contribution of the cofactors, of the polypeptide backbone and of several specific residues of both enzymes. It was observed that the FAD is in a more hydrophobic environment in the *T. thermophilus* enzyme than in its *E. coli* homologue, and that an acidic residue in a highly hydrophobic environment is protonated upon reduction. This core might play a role in protecting the FAD at high temperature. These observations suggest a higher hydrophobicity of the catalytic center of the *T. thermophilus* enzyme.

The temperature-dependent FTIR study clearly demonstrates the denaturation and aggregation of the *E. coli* SQR at temperatures above 50 °C, which correlates well with the decrease in activity observed for this enzyme at this temperature. The *T. thermophilus* homologue, in contrast, does not exhibit any major structural changes at temperatures up to

80 °C. Only minor conformational changes which result in a partial opening of the protein to the solvent occur. Despite these internal movements, a hydrophobic core still remains in this protein at 80 °C. Thermostability in this enzyme thus seems to result from both a reduction in the number of turns and a stronger hydrophobic core.

Experimental Section

Protein expression and purification: The SQOR from *E. coli*[13] and the monomeric His-tagged variant of SQOR from *T. thermophilus*[17] were purified as previously reported.

Electrode preparation: A commercial glassy carbon disk electrode (3 mm diameter) was polished to a mirror-like finish with 4 μm diamond paste and sonicated in water and absolute ethanol. Then 10 μl of a dispersion of SWNTs in EtOH/water mixture were deposited on the electrode surface and allowed to dry under air. Two other deposits of SWNTs were made. The electrode was then heated at 100 °C for two hours and cooled down to room temperature. Prior to adsorption, the stock solutions of detergent-solubilized protein were washed with 50 mM phosphate pH 8 buffer solution without detergent in a 100 kDa centrifugal filter unit. The electrode surface was incubated overnight at 4 °C with 4 μl of the protein solution. The electrode was finally rinsed with fresh buffer to remove excess protein.

Characterization by Raman spectroscopy: The adsorption of the protein on the SWNTs was followed by Raman spectroscopy using a Renishaw Invia Raman Microscope operating at 514 nm. The dispersion of SWNTs was deposited on a CaF_2 window and allowed to dry before addition of 6 μl of the protein solution. The excess of protein was then removed by gentle rinsing with fresh buffer. Typically, 5 spectra obtained with 15 s irradiation time and 25 mW laser power were averaged.

Atomic force microscopy (AFM) was performed using a Veeco Multimode Nanoscope V (Brucker) to characterize the topography of the coated electrodes. The images were obtained in contact mode in dry condition with silicon nitride cantilever with a spring constant of 0.6 N/m (model MSCT-AUHW, Veeco, CA). Deflection and height mode images were scanned simultaneously at a fixed scan rate (1 Hz) with a resolution of 512 × 512 pixels. The average roughness of the deposited films, corresponding to the root mean square values given by the Nanoscope software, was determined from 5 different areas of 5 × 5 μm^2.

Electrochemical studies: CV measurements were performed in a standard three electrode cell connected to a Princeton Applied Research VERSASTAT 4 potentiostat. An aqueous AgCl/Ag 3M NaCl electrode was used as reference electrode and a platinum wire as counter electrode. The voltammograms were obtained at different temperatures in Ar-flushed 50 mM phosphate pH 8 buffer solution containing 4 mM sodium succinate. The potentials are quoted versus the standard reference electrode.

Electrochemically-induced FTIR difference spectroscopy: FTIR difference spectra were recorded at 10°C as a function of the applied potential in an Optically Transparent Thin Layer Electrochemical cell described previously.[74] A gold grid served as working electrode. To accelerate the redox reaction, 16 different mediators were added at a final concentration of 15 μM.[29] The cell was placed in the sample compartment of a Vertex 70

FTIR spectrometer from Bruker. The measurements were performed in the mid infrared domain using a globar source and a KBr beamsplitter. First, the protein was equilibrated at −0.40 V vs SHE for 5 minutes and a single-beam spectrum was recorded. Then a potential of 0.20 V was applied, and a single-beam spectrum was again recorded after 5 minutes. Difference spectra were calculated from two single-beam spectra, with the initial spectrum taken as reference. Typically, 256 interferograms at 4 cm^{-1} resolution were coadded for each single-beam spectrum, and Fourier transformed using triangular apodization and a zero filling factor of 2. 20–30 difference spectra were averaged.

Temperature-dependent FTIR spectroscopy: prior to measurements, H_2O to D_2O exchange was performed by washing three times the protein sample with phosphate buffer in D_2O (pD 8) on a microcon. The protein was then equilibrated for a few hours in pD 8 phosphate buffer at 5 °C to let the deuteration of the protein occur. Then 3 μl of the protein solution in D_2O were placed between two CaF_2 windows in the sample compartment of a Vertex 70 spectrometer from Bruker. The temperature was adjusted with a thermostat. An equilibrium time of 20 minutes was chosen. Typically 256 scans at a resolution of 4 cm^{-1} were averaged. The final spectra were corrected from the contribution of humidity and smoothed to 5 points.

Supplementary Material

Refer to Web version on PubMed Central for supplementary material.

Acknowledgements

P. H. and F. M. are grateful to the International Center for Frontier Research in Chemistry in Strasbourg (RTRA) for the financial support for the Raman equipment. P. H. is grateful to the Institut Universitaire de France (IUF) and the FRC. G.C. thanks National Institutes of Health GM61606 and the Department of Veterans Affairs BX001077 for support. E. P. was supported by a Labex NIE project (Strasbourg, France). Part of the work was funded by the Irish Research Council (M.R.N.)

References

1. Hederstedt, L.; Ohnishi, T. New Comprehensive Biochemistry. Lars, E., editor. Vol. 23. Elsevier; 1992. p. 163-198.
2. Hägerhäll C. Biochim. Biophys. Acta. 1997; 1320:107–141. [PubMed: 9210286]
3. Lancaster, CRD. Handbook of Metalloproteins. Messerschmidt, A., editor. Vol. 1. John Wiley & Sons Ltd.; 2001. p. 379-401.
4. Cecchini G, Schröder I, Gunsalus RP, Maklashina E. Biochim. Biophys. Acta. 2002; 1553:140–157. [PubMed: 11803023]
5. Lancaster CRD. Biochim. Biophys. Acta. 2002; 1553:1–6. [PubMed: 11803013]
6. Cecchini G. Annu. Rev. Biochem. 2003; 72:77–109. [PubMed: 14527321]
7. Lancaster, CRD. Encyclopedia of Biological Chemistry. Lennarz, WJ.; Lane, MD., editors. New York: Elsevier; 2004. p. 681-687.
8. Maklashina E, Cecchini G. Biochim. Biophys. Acta. 2010; 1797:1877–1882. [PubMed: 20175986]
9. Iverson TM, Luna-Chavez C, Cecchini G, Rees DC. Science. 1999; 284:1961–1966. [PubMed: 10373108]
10. Lancaster CRD, Kröger A, Auer M, Michel H. Nature. 1999; 402:377–385. [PubMed: 10586875]
11. Yankovskaya V, Horsefield R, Törnroth S, Luna-Chavez C, Miyoshi H, Léger C, Byrne B, Cecchini G, Iwata S. Science. 2003; 299:700–704. [PubMed: 12560550]

12. Horsefield R, Yankovskaya V, Sexton G, Whittingham W, Shiomi K, Ōmura S, Byrne B, Cecchini G, Iwata S. J. Biol. Chem. 2006; 281:7309–7316. [PubMed: 16407191]
13. Ruprecht J, Yankovskaya V, Maklashina E, Iwata S, Cecchini G. J. Biol. Chem. 2009; 284:29836–29846. [PubMed: 19710024]
14. Huang, L-s; Sun, G.; Cobessi, D.; Wang, AC.; Shen, JT.; Tung, EY.; Anderson, VE.; Berry, EA. J. Biol. Chem. 2006; 281:5965–5972. [PubMed: 16371358]
15. Sun F, Huo X, Zhai Y, Wang A, Xu J, Su D, Bartlam M, Rao Z. Cell. 2005; 121:1043–1057. [PubMed: 15989954]
16. Kolaj-Robin O, O'Kane SR, Nitschke W, Léger C, Baymann F, Soulimane T. Biochim. Biophys. Acta. 2011; 1807:68–79. [PubMed: 20951673]
17. Kolaj-Robin O, Noor MR, O'Kane SR, Baymann F, Soulimane T. PLoS One. 2013; 8:e53559. [PubMed: 23308253]
18. Querol E, Perez-Pons JA, Mozo-Villarias A. Protein Eng. 1996; 9:265–271. [PubMed: 8736493]
19. Kumar S, Tsai C-J, Nussinov R. Protein Eng. 2000; 13:179–191. [PubMed: 10775659]
20. Szilágyi A, Závodszky P. Structure. 2000; 8:493–504. [PubMed: 10801491]
21. Kumar S, Nussinov R. Cell. Mol. Life Sci. 2001; 58:1216–1233. [PubMed: 11577980]
22. Sadeghi M, Naderi-Manesh H, Zarrabi M, Ranjbar B. Biophys. Chem. 2006; 119:256–270. [PubMed: 16253416]
23. Pershad HR, Hirst J, Cochran B, Ackrell BAC, Armstrong FA. Biochim. Biophys. Acta. 1999; 1412:262–272. [PubMed: 10482788]
24. Sucheta A, Ackrell BAC, Cochran B, Armstrong FA. Nature. 1992; 356:361–362. [PubMed: 1549182]
25. Sucheta A, Cammack R, Weiner J, Armstrong FA. Biochemistry. 1993; 32:5455–5465. [PubMed: 8499449]
26. Jeuken LJC, Jones AK, Chapman SK, Cecchini G, Armstrong FA. J. Am. Chem. Soc. 2002; 124:5702–5713. [PubMed: 12010043]
27. Hudson JM, Heffron K, Kotlyar V, Sher Y, Maklashina E, Cecchini G, Armstrong FA. J. Am. Chem. Soc. 2005; 127:6977–6989. [PubMed: 15884941]
28. Turner KL, Doherty MK, Heering HA, Armstrong FA, Reid GA, Chapman SK. Biochemistry. 1999; 38:3302–3309. [PubMed: 10079073]
29. Maklashina E, Hellwig P, Rothery RA, Kotlyar V, Sher Y, Weiner JH, Cecchini G. J. Biol. Chem. 2006; 281:26655–26664. [PubMed: 16829675]
30. Haas AH, Sauer US, Gross R, Simon J, Mäntele W, Lancaster CRD. Biochemistry. 2005; 44:13949–13961. [PubMed: 16229484]
31. Mileni M, Haas AH, Mäntele W, Simon J, Lancaster CRD. Biochemistry. 2005; 44:16718–16728. [PubMed: 16342962]
32. Wille G, Ritter M, Friedemann R, Mäntele W, Hübner G. Biochemistry. 2003; 42:14814–14821. [PubMed: 14674755]
33. Neehaul Y, Juárez O, Barquera B, Hellwig P. Biochemistry. 2013; 52:3085–3093. [PubMed: 23566241]
34. Berthomieu C, Boussac A, Maentele W, Breton J, Nabedryk E. Biochemistry. 1992; 31:11460–11471. [PubMed: 1332761]
35. Hellwig P, Soulimane T, Buse G, Mantele W. Biochemistry. 1999; 38:9648–9658. [PubMed: 10423243]
36. El Khoury Y, Trivella A, Gross J, Hellwig P. Chem Phys Chem. 2010; 11:3313–3319. [PubMed: 20737532]
37. Hellwig P, Behr J, Ostermeier C, Richter O-MH, Pfitzner U, Odenwald A, Ludwig B, Michel H, Mäntele W. Biochemistry. 1998; 37:7390–7399. [PubMed: 9585553]
38. Lübben M, Prutsch A, Mamat B, Gerwert K. Biochemistry. 1999; 38:2048–2056. [PubMed: 10026287]
39. Barth A. Biochim. Biophys. Acta. 2007; 1767:1073–1101. [PubMed: 17692815]
40. Davis JJ, Coles RJ, Allen H, Hill O. J. Electroanal. Chem. 1997; 440:279–282.

41. Wang G, Xu J-J, Chen H-Y. Electrochem. Commun. 2002; 4:506–509.
42. Wang J, Li M, Shi Z, Li N, Gu Z. Anal. Chem. 2002; 74:1993–1997. [PubMed: 12033297]
43. Gooding JJ, Wibowo, Liu R, Yang W, Losic D, Orbons S, Mearns FJ, Shapter JG, Hibbert DB. J. Am. Chem. Soc. 2003; 125:9006–9007. [PubMed: 15369344]
44. Katz E, Willner I. ChemPhysChem. 2004; 5:1084–1104. [PubMed: 15446731]
45. Patolsky F, Weizmann Y, Willner I. Angew. Chem. Int. Ed. 2004; 43:2113–2117.
46. Gao F, Viry L, Maugey M, Poulin P, Mano N. Nat. Commun. 2010; 1:2. [PubMed: 20975669]
47. Silveira CM, Baur J, Holzinger M, Moura JJG, Cosnier S, Almeida MG. Electroanal. 2010; 22:2973–2978.
48. Zebda A, Gondran C, Le Goff A, Holzinger M, Cinquin P, Cosnier S. Nat. Commun. 2011; 2:370. [PubMed: 21712818]
49. Pelster LN, Minteer SD. Electrochim. Acta. 2012; 82:214–217.
50. Lalaoui N, Elouarzaki K, Goff AL, Holzinger M, Cosnier S. Chem. Commun. 2013; 49:9281–9283.
51. Tans SJ, Devoret MH, Dai H, Thess A, Smalley RL, Geerligs LJ, Dekker C. Nature. 1997; 386:474–477.
52. Pumera M. Chem. Eur. J. 2009; 15:4970–4978. [PubMed: 19360829]
53. Dresselhaus MS, Dresselhaus G, Saito R, Jorio A. Phys. Rep. 2005; 409:47–99.
54. Dresselhaus MS, Jorio A, Hofmann M, Dresselhaus G, Saito R. Nano Lett. 2010; 10:751–758. [PubMed: 20085345]
55. Spiro TG. Phys. Bioinorg. Chem. Ser. 1983; 2:89–159.
56. Kitagawa, T.; Ozaki, Y. Metal Complexes with Tetrapyrrole Ligands I. Buchler, J., editor. Vol. 64. Springer Berlin Heidelberg; 1987. p. 71-114.
57. Parthasarathi N, Hansen C, Yamaguchi S, Spiro TG. J. Am. Chem. Soc. 1987; 109:3865–3871.
58. Yachandra VK, Hare J, Gewirth A, Czernuszewicz RS, Kimura T, Holm RH, Spiro TG. J. Am. Chem. Soc. 1983; 105:6462–6469.
59. Mino Y, Loehr TM, Wada K, Matsubara H, Sanders-Loehr J. Biochemistry. 1987; 26:8059–8065. [PubMed: 3442645]
60. Sanders-Loehr, J. Metal Clusters in Proteins. Vol. 372. American Chemical Society; 1988. p. 49-67.
61. Han S, Czernuszewicz RS, Kimura T, Adams MWW, Spiro TG. Journal of the American Chemical Society. 1989; 111:3505–3511.
62. Han S, Czernuszewicz RS, Kimura T, Adams MWW, Spiro TG. J. Am. Chem. Soc. 1989; 111:3505–3511.
63. Kita K, Vibat CR, Meinhardt S, Guest JR, Gennis RB. J. Biol. Chem. 1989; 264:2672–2677. [PubMed: 2644269]
64. Ruprecht J, Iwata S, Rothery RA, Weiner JH, Maklashina E, Cecchini G. J. Biol. Chem. 2011; 286:12756–12765. [PubMed: 21310949]
65. Susi H, Timasheff SN, Stevens L. J. Biol. Chem. 1967; 242:5460–5466. [PubMed: 12325360]
66. Jackson M, Haris PI, Chapman D. J. Mol. Struct. 1989; 214:329–355.
67. Haris PI, Chapman D. Trends Biochem. Sci. 1992; 17:328–333. [PubMed: 1412707]
68. Goormaghtigh, E.; Cabiaux, V.; Ruysschaert, J-M. Physicochemical Methods in the Study of Biomembranes. Hilderson, H.; Ralston, G., editors. Vol. 23. Springer US; 1994. p. 405-450.
69. Arrondo JLR, Young NM, Mantsch HH. Biochim. Biophys. Acta. 1988; 952:261–268. [PubMed: 3337827]
70. Muga A, Arrondo JLR, Bellon T, Sancho J, Bernabeu C. Arch. Biochem. Biophys. 1993; 300:451–457. [PubMed: 8424679]
71. Haltia T, Semo N, Arrondo JLR, Goni FM, Freire E. Biochemistry. 1994; 33:9731–9740. [PubMed: 8068652]
72. Thompson MJ, Eisenberg D. J. Mol. Biol. 1999; 290:595–604. [PubMed: 10390356]
73. Oshima T, Imahori K. Int. J. Syst. Bacteriol. 1974; 24:102–112.

74. Moss D, Nabedryk E, Breton J, Mäntele W. Eur. J. Biochem. 1990; 187:565–572. [PubMed: 2154376]

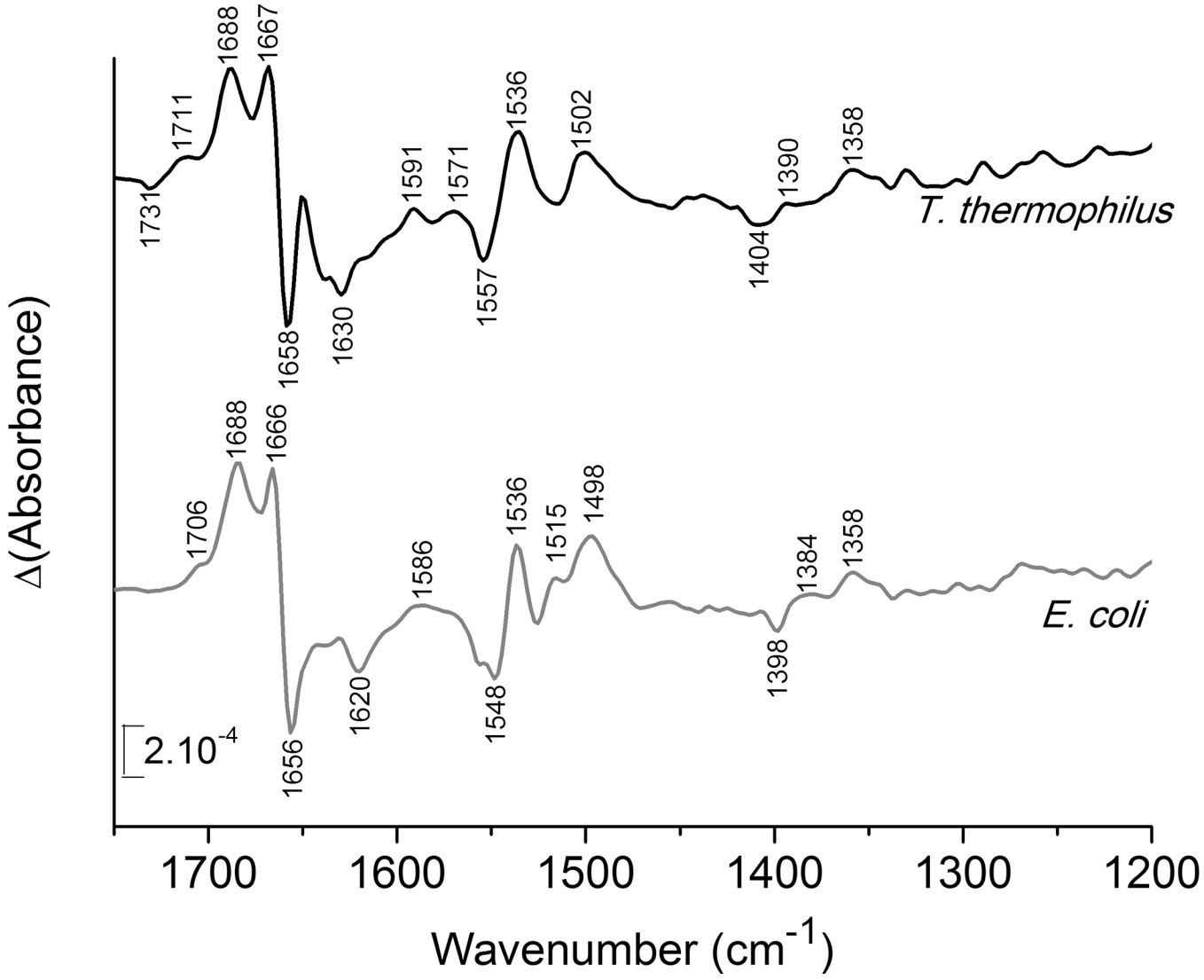

Figure 1.

Oxidized-minus-reduced FTIR difference spectra of *T. thermophilus* (monomeric variant) and *E. coli* SQRs at pH 8 for a potential step from −0.4 to 0.2 V.

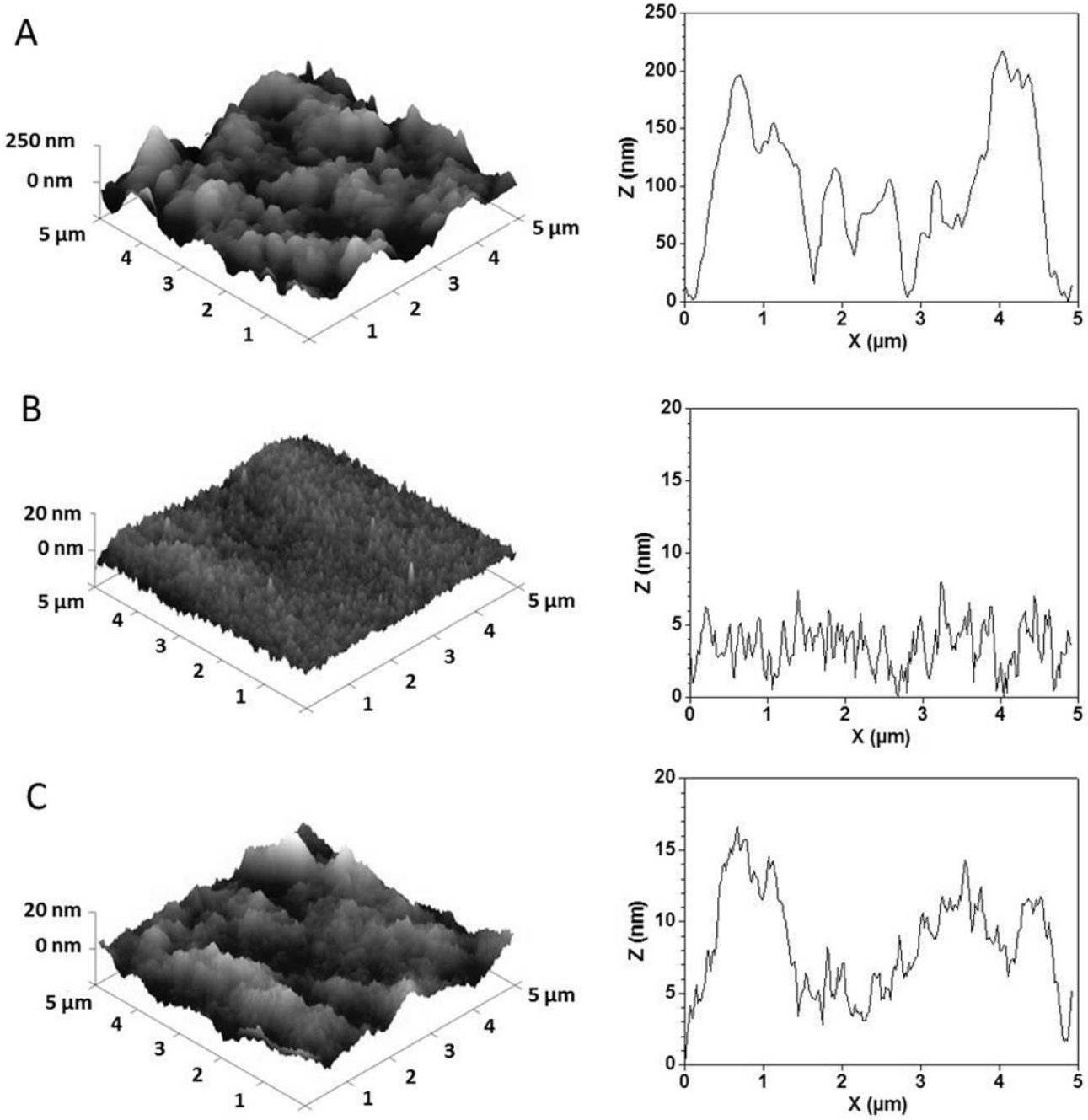

Figure 2.

Topography (left) and profilometric section (right), obtained by AFM in contact mode and dry condition, for (A) SWNTs-coated glassy carbon substrates, (B) E. coli SQR deposited on SWNTs-coated glassy carbon substrates and (C) T. thermophilus SQR deposited on SWNTs-coated glassy carbon substrates.

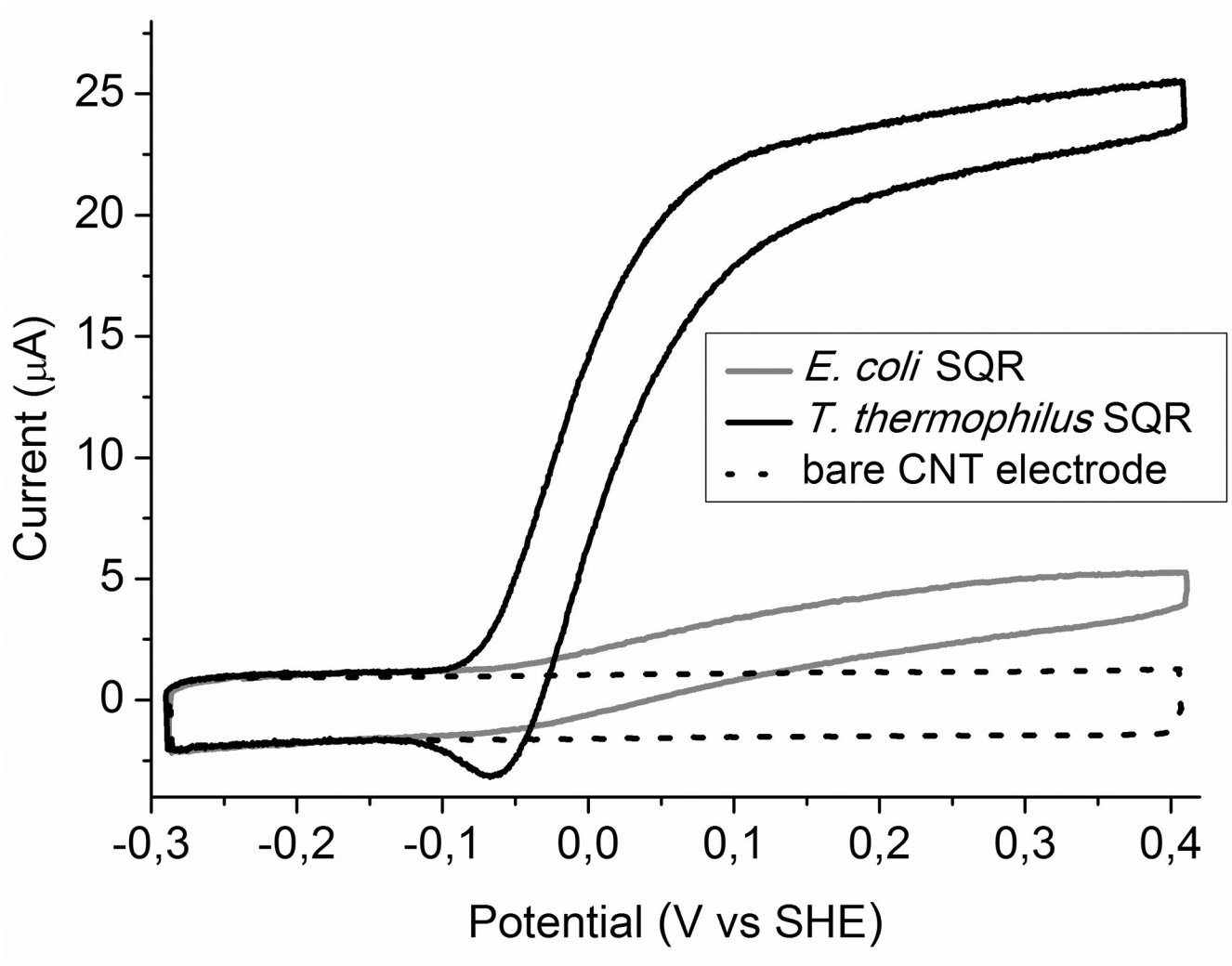

Figure 3.
Cyclic voltammetry of SQR from *E. coli* (solid grey trace) and *T. thermophilus* (solid black trace) immobilized on SWNTs-modified glassy carbon electrodes in phosphate pH 8 buffer containing 4 mM sodium succinate at 20 °C. Scan rate: 2 mV/s.

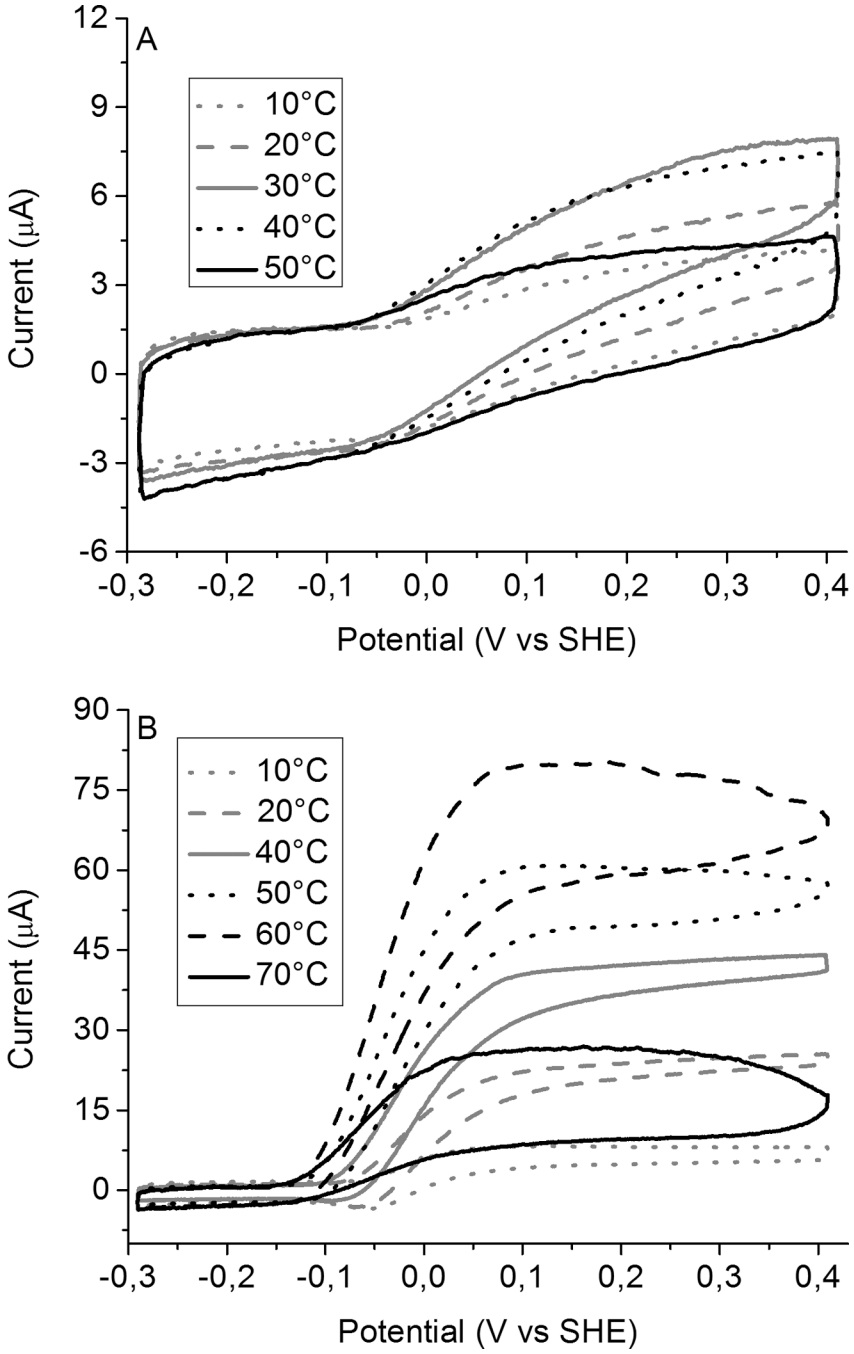

Figure 4.

Temperature-dependent cyclic voltammetry of SQR from *E. coli* (A) and *T. thermophilus* (B) immobilized on SWNTs modified electrodes in phosphate pH 8 buffer containing 4 mM sodium succinate. Scan rate: 2 mV/s

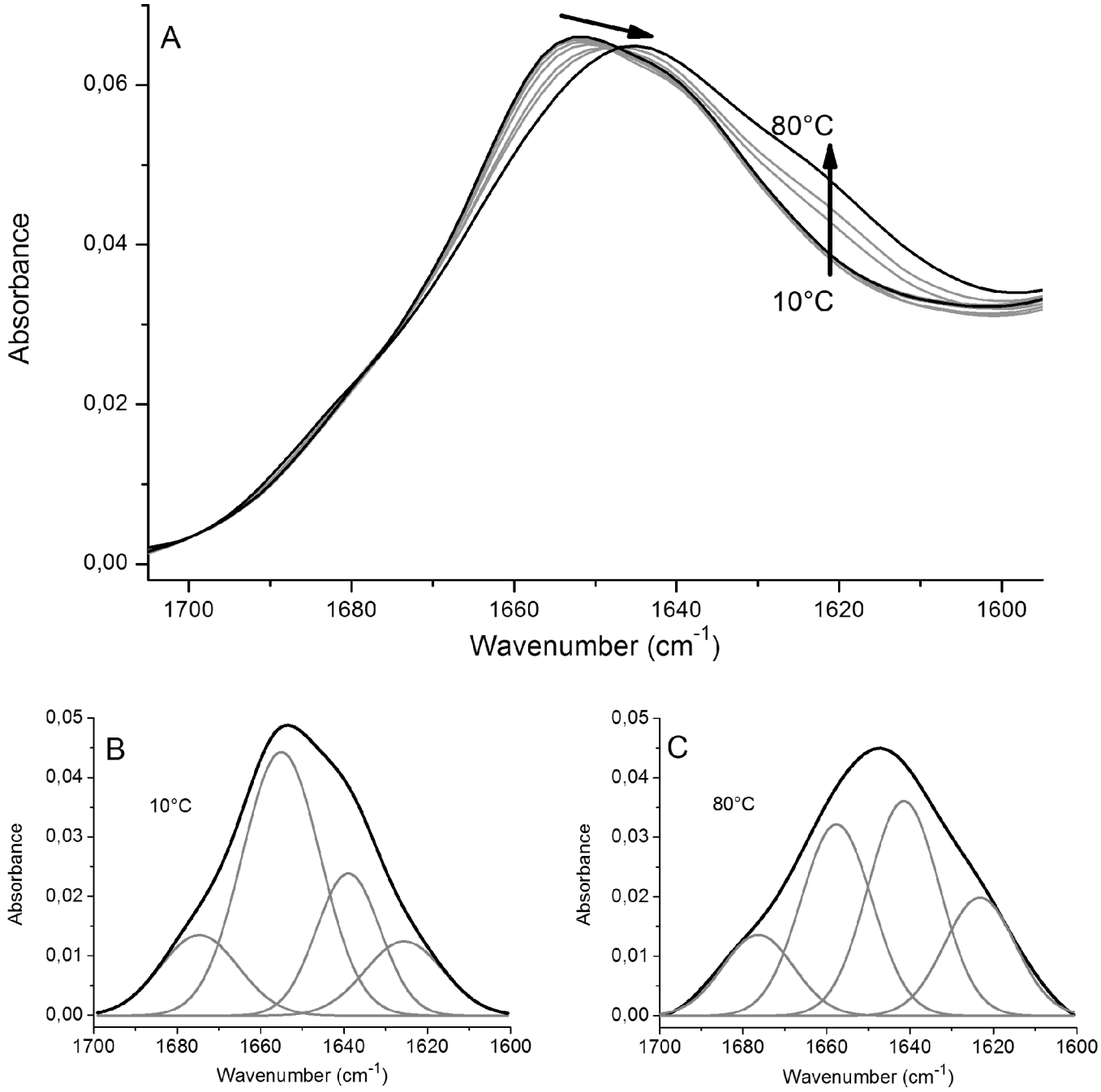

Figure 5.

Temperature-dependent FTIR spectra of *E. coli* SQR obtained at pD 8 (A) and deconvolution of the band at 10 °C (B) and 80 °C (C).

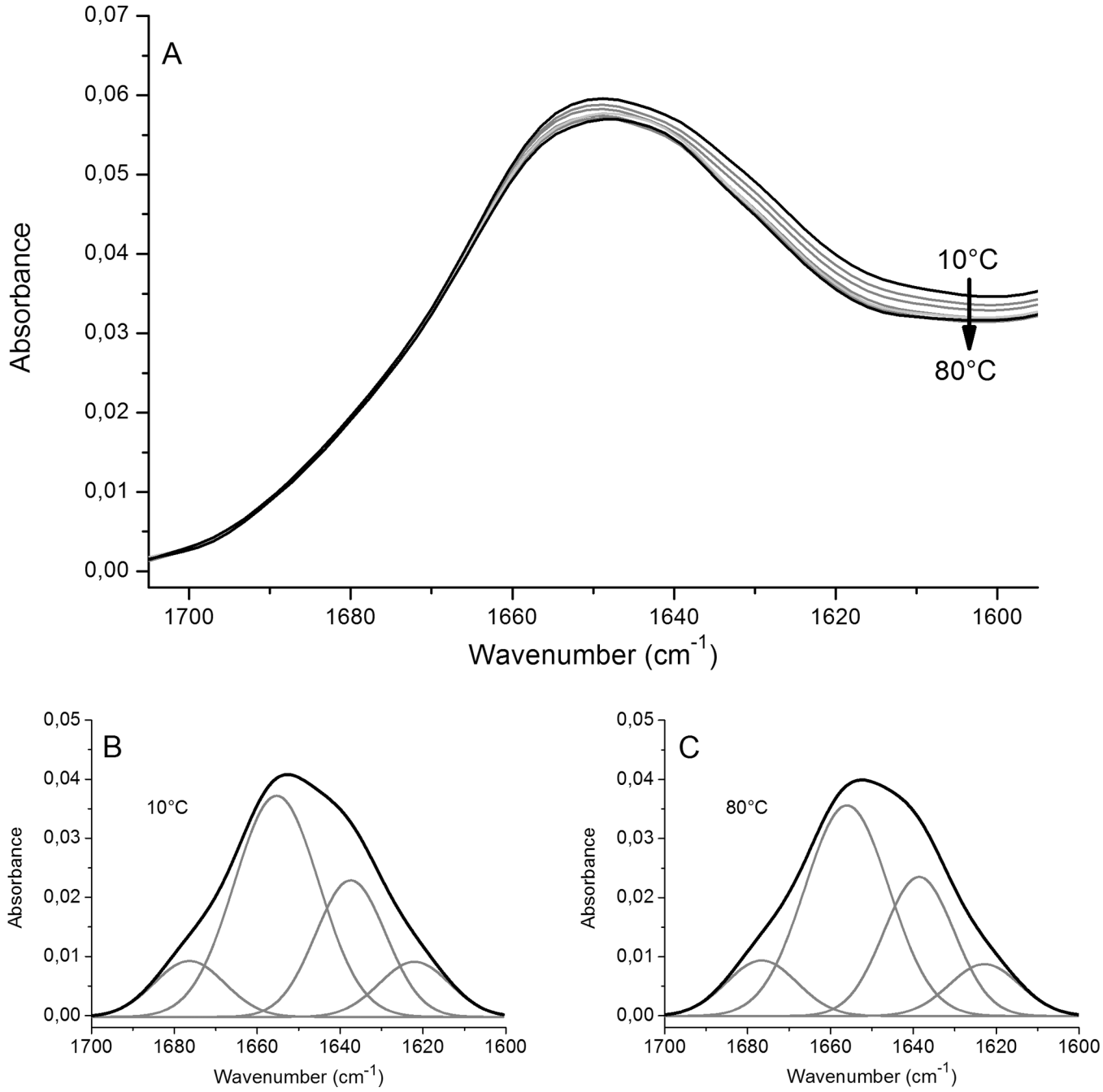

Figure 6.
Temperature-dependent FTIR spectra of *T. thermophilus* SQR obtained at pD 8 (A) and deconvolution of the band at 10 °C (B) and 80 °C (C).

Table 1

Secondary structure analysis of the *E. coli* and *T. thermophilus* SQRs at 10 and 80 °C

SQR	Temp.	α-helix[a]	β-sheets +random[b]	turns[c]
E. coli	10 °C	49%	37%	14%
	80 °C	32%	55%	13%
T. thermophilus	10 °C	52%	37%	11%
	80 °C	51%	38%	11%

[a] 1648–1658 cm^{-1}

[b] 1620–1640 cm^{-1}

[c] 1665–1690 cm^{-1}